

pubs.acs.org/Macromolecules Article

Emergence of Disordered Hyperuniformity in Melts of Linear Diblock Copolymers

Duyu Chen,* Michael A. Klatt, and Glenn H. Fredrickson*



Cite This: *Macromolecules* 2024, 57, 9911–9919



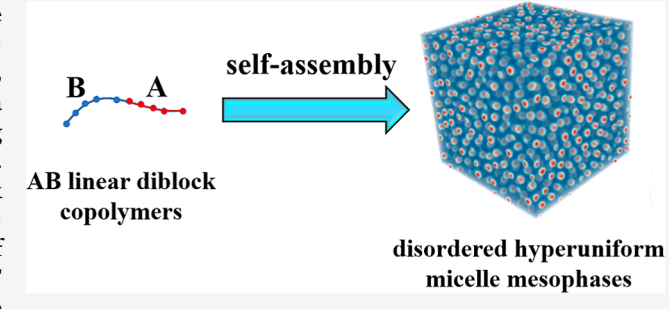
ACCESS I

III Metrics & More

Article Recommendations

Supporting Information

ABSTRACT: Disordered hyperuniform (DHU) systems are recently discovered exotic states of matter, where (normalized) infinite-wavelength density fluctuations are completely suppressed, as in crystals, even though the systems are isotropic and lack a conventional long-range order. Despite recent success, realizing such systems using bottom-up approaches remains challenging. Here, we study the DHU properties of neat melts of linear diblock copolymers by using large-cell self-consistent field theory (SCFT) simulations. We initialize SCFT simulations using a wide variety of disordered point patterns and upon relaxation via a SCFT algorithm obtain a new class of metastable disordered micelle



mesophases that are hyperuniform. The final relaxed structures are independent of the specific type of initial disorder used to seed the SCFT simulations, but simulations initialized using point patterns that correspond to the local energy minimum of the so-called Quantizer energy, a geometric functional related to the free energy of copolymeric self-assemblies, possess the fastest convergence. Moreover, we find that DHU micelle mesophases possess free energies very similar to those of the thermodynamically stable body-centered cubic sphere mesophases and are also more favorable energetically than previously obtained liquid-like packings. Our findings shed light on the design of novel disordered hyperuniform materials using bottom-up approaches and suggest new possibilities for technological applications such as novel noniridescent structural colors.

■ INTRODUCTION

Disordered hyperuniform (DHU) systems are recently discovered exotic states of matter^{1,2} that have features common to both perfect crystals and liquids. These systems are similar to liquids or glasses in that they are statistically isotropic and possess no Bragg peaks, i.e., they lack a conventional longrange translational and orientational order; nevertheless, they completely suppress (normalized) infinite-wavelength density fluctuations, like crystals, and in this sense, they possess a hidden long-range order. 1-3 In particular, DHU many-body systems in d-dimensional Euclidean space \mathbb{R}^d are characterized by a vanishing structure factor S(k) in the infinite-wavelength limit, i.e., $\lim_{k\to 0} S(k) = 0$, where k is the wavenumber.^{1,2} Equivalently, these systems can be characterized by a vanishing normalized local number variance $\sigma^2(R)/R^d$ in the large-R limit, where $\sigma^2(R) \equiv \langle N^2(R) \rangle - \langle N(R) \rangle^2$ is the local number variance associated with a spherical window of radius R, N(R)denotes the number of particles in a spherical window of radius R randomly placed into the system, and $\langle \cdots \rangle$ denotes an ensemble average. 1,2 DHU states have been discovered in a variety of equilibrium and nonequilibrium physical and biological systems, and their exotic structural features have been shown to endow such systems with desirable physical properties that cannot be achieved in either ordinary disordered or perfectly crystalline states. 1,2,4-15 For example, certain DHU dielectric networks^{4,16} were found to possess complete photonic band gaps comparable in size to photonic crystals, while at the same time maintaining statistical isotropy, enabling waveguide geometries not possible with photonic crystals.⁵ Today, most DHU materials are designed "top-down" since a realization via "bottom-up" self-assembly remains challenging,² despite a few such examples.^{17,18}

Recently, Chremos and Douglas¹⁹ have found that the cores of star polymers and the backbones of bottlebrush polymers possess a hyperuniform distribution in their melts, although the mesophases formed by these star and bottlebrush polymers overall are not hyperuniform. In a recent work, ²⁰ some of us have demonstrated that point patterns corresponding to the local potential-energy minima associated with the "Quantizer energy" (defined as the sum of the moment of inertia of each Voronoi cell) are effectively hyperuniform. Interestingly, this Quantizer energy is reminiscent of the entropic chain stretching free energy of copolymeric self-assemblies. ^{21,22} For

Received: July 29, 2024
Revised: September 20, 2024
Accepted: September 26, 2024

Published: October 3, 2024





example, in the diblock foam model of block copolymer melts,²² the free energy is expressed as a weighted sum of an interfacial energy term and the Quantizer energy. These earlier results motivated the search for disordered hyperuniform mesophases in block copolymer systems.

While the equilibrium mesophases of block copolymers are well studied by theory and experiment, ^{23,24} the self-assembly of block copolymers has sometimes been observed to suffer from slow dynamics, making it difficult to achieve the true equilibrium state. ^{25,26} In particular, near the order—disorder transition (ODT), upon rapid cooling from the disordered homogeneous state, systems are often kinetically trapped into a mysterious "liquid-like" packing (LLP) state, whose scattering pattern typically exhibits a broad peak and lacks the sharp Bragg peaks associated with ordered morphologies. ^{27–30} This LLP state also exhibits essentially solid-like mechanical properties while maintaining a disordered morphology and thus may be thought of as a soft glass. ²⁹ However, it is currently unclear from the available experimental data whether these disordered packings are hyperuniform or nonhyperuniform.

Using large-cell self-consistent field theory (SCFT) simulations initialized from the structure of a Lennard-Jones fluid, Dorfman and Wang³¹ recently demonstrated that compositionally asymmetric diblock copolymers possess a rugged free energy landscape with vast numbers of metastable liquid-like states corresponding to distinct aperiodic packings of spherical micelles. They further postulated that this vast population of near-degenerate liquid-like states is responsible for the slow ordering kinetics. However, the number of spheres employed in the SCFT simulations was relatively small (54 micelles), so questions regarding the nature of the disordered liquid state at large length scales remain unanswered, specifically whether such structures are DHU in character. We note that previous SCFT simulations³² have been used to probe the properties of disordered mesophases in melts of compositionally symmetric linear AB diblock copolymers as well.

Here, we show, for the first time, that DHU mesophases are energetically competitive in neat melts of block copolymers and, to this end, establish a link between the two research fields of disordered hyperuniform systems and block copolymers. In particular, we obtain a class of metastable mesophases consisting of disordered A-rich micelle cores distributed in a continuous B-rich matrix in neat melts of AB linear diblock copolymers. Specifically, we first develop a Gaussian kernel method to initialize SCFT simulations of disordered micelles using a wide variety of disordered point patterns, in particular those corresponding to local energy minima of the Quantizer energy with respect to micelle centers. To evaluate the largewavelength density fluctuations, we then perform large-cell SCFT simulations containing as many as 2000 micelles in the simulation box and obtain metastable mesophases that are local free energy minima. Importantly, we find that these mesophases are DHU, which distinguishes them from typical liquid or glass morphologies. Moreover, these metastable mesophases possess very similar free energies to the thermodynamically stable BCC sphere phase (with free energy $1.0003 \times F_{BCC}$) and are approximately 60% lower in free energy relative to the BCC sphere phase than previously obtained³¹ liquid-like packings. Our findings suggest a new bottom-up route to realize DHU materials.

RESULTS

Initialization of SCFT. The micelles formed by block copolymers often contain a large number of polymer chains, and each polymer chain typically consists of a large number of atoms. This makes it computationally difficult or intractable to study copolymer mesophases using all-atom or even coarsegrained particle-based simulations over time scales relevant to the self-assembly of block copolymers.³³ Fortunately, exact mathematical transformations exist that can decouple the many-body interactions among polymer chains and replace them with independent interactions between a single polymer chain and one or more auxiliary potential fields $w(\mathbf{r})$.³³ Among these field-based simulations, SCFT simulations ³³ are ones based on a mean-field approximation and over the past few decades have enjoyed considerable success in predicting the self-assembly behavior of various block copolymer systems [see Supporting Information for a brief introduction to SCFT simulations]. In this work, we employ discrete Gaussian chain models for the incompressible melts of AB linear diblock copolymers. The segmental interactions are described by a Flory-Huggins interaction parameter χ that favors similar monomer contacts (A–A and B–B) over dissimilar contacts (A–B). It is well-known at the mean-field (or SCFT) level that the equilibrium phase behavior of conformationally symmetric AB linear diblock copolymers is dictated by the volume fraction f_A of the minority monomer species of A and segregation strength χN , where N is the degree of polymerization for a polymer chain. On the other hand, the effect of temperature on the phase behavior is taken into account via χ as χ typically has temperature dependence $\chi(T) = A/T + B$ with A > 0.33 Here, B is a constant and T is the temperature. Since the exact value of χ also depends on the specific types of monomer species, the dependence of phase behavior on temperature is not universal.

To model disordered micelle mesophases, we initialized the SCFT simulations using different disordered point patterns as initial sphere locations via a Gaussian kernel method that we have developed. Specifically, we first run a unit-cell simulation for a BCC sphere phase and extract the converged values $w_{i,\text{in}}$ and $w_{i,\text{out}}$ for each auxiliary field $w_i(\mathbf{r})$ at the maximum and minimum of the density field $\rho_{\rm A}(\mathbf{r})$ of the micelle-forming monomer species A, respectively. Here, the maximum of the density field $\rho_{\rm A}(\mathbf{r})$ is deep inside a micelle, while the minimum is deep within the B-rich matrix, and we assume that A is the minority species with an average volume fraction of A segments, $f_{\rm A}$, smaller than 1/2. Subsequently, we generate the initial guess for each auxiliary field according to

$$w_i(\mathbf{r}) = w_{i,\text{in}} \exp\left(-\frac{d(\mathbf{r})^2}{R^2}\right) + w_{i,\text{out}} \left[1 - \exp\left(-\frac{d(\mathbf{r})^2}{R^2}\right)\right]$$
(1)

where $d(\mathbf{r})$ is the shortest distance between the grid point \mathbf{r} and any of the prescribed sphere centers, and the effective radius R of a micelle is given by $R = \left(\frac{f_{\rm A}V}{N_{\rm s}4\pi/3}\right)^{1/3}$, where V is the volume of the simulation box and $N_{\rm s}$ is the number of micelles in the box. In this work, we adopt the multispecies exchange model³⁴ and explicitly track $w_{\rm A}(\mathbf{r})-w_{\rm B}(\mathbf{r})$ and $w_{\rm B}(\mathbf{r})$ in our simulations.

We considered a variety of disordered point patterns as initial sphere locations, including:

- Quantizer point patterns: Roughly speaking, the Quantizer problem is defined as the optimization of the moment of inertia of Voronoi cells, i.e., similarly sized sphere-like polyhedra that tile space are preferred. Specifically, for a given set of n "generating" points z_1 , ..., \mathbf{z}_n , the Voronoi partition is the partition of space into cells, where each Voronoi cell C_i consists of all points in space that are closer to \mathbf{z}_i than to any other point $\mathbf{z}_{i\neq i}$. The "Quantizer energy" is the total energy $\sum_{i} E(C_{i}, \mathbf{z}_{i})$ summing up all individual cell contributions, and the cell energy $E(C_i, \mathbf{z}_i)$ is given by $E(C_i, \mathbf{z}_i) \equiv \int_{C_i} ||\mathbf{x} - \mathbf{z}_i||^2 d\mathbf{x}$. We employ Lloyd's algorithm to obtain local energy minima of the Quantizer energy. Lloyd's algorithm can be viewed as a gradient descent algorithm that minimizes the total energy $\sum_{i} E(C_{i}, \mathbf{z}_{i})$ with respect to the set of generating positions $\{z_i\}$. In each step of the algorithm, a Voronoi tessellation based on the generating points subject to periodic boundary conditions is generated, and the center of mass of each Voronoi cell is determined. Then, the generating points are moved to the centers of mass, based on which a new tessellation is generated. This process is repeated until the generating points converge to the centers of mass. Thus, a centroidal Voronoi tessellation³⁵ is obtained. When disordered configurations are used as initial conditions for Lloyd's algorithm, the final configurations are also disordered but possess effective hyperuniformity.
- Poisson point patterns: These patterns are completely random configurations of snapshots of the ideal gas in the canonical ensemble, where the particle coordinates are independently and uniformly distributed in the simulation box.
- Hard-sphere liquids: We generate equilibrium packings of monodisperse, frictionless, hard spheres (i.e., balls that are impenetrable but do not interact otherwise) at packing fraction $\phi \approx 0.25$, which are well-known to be liquids that are nonhyperuniform, i.e., their structure factor S(k) extrapolates to S_0 as k goes to zero, where S_0 is a positive constant on the order of 10^{-1} or 10^{-2} .
- Random close packings: These are jammed, non-equilibrium packings of monodisperse frictionless hard spheres at packing fraction $\phi \approx 0.64$, which we generate using the Lubachevsky–Stillinger algorithm.³⁶
- Disordered stealthy hyperuniform point patterns: These are disordered, statistically isotropic point configurations, for which the structure factor vanishes not only at an infinite wavelength (i.e., at k=0) but at all wavelengths above a finite threshold (i.e., for a finite range of wavenumbers $k < k_0$ where $k_0 > 0$). We obtain such point patterns with a degree of stealthiness $\chi = 0.49$ (not to be confused with the Flory–Huggins parameter χ) using the procedure described in a previous work, where χ is the fraction of the number of constrained independent k points over the total number of degrees of freedom (subtracting out the system translational degrees of freedom).

For each type of point pattern, we generate 10 configurations at system size $N_{\rm s}=2000$ points, and for the point patterns associated with the local energy minima of the Quantizer energy (which we used for most of the results in this work), we also generate 10 configurations at $N_{\rm s}=432$ to study the system size effect. We find that the seeds for the micelles

generated using this Gaussian kernel method typically converge quickly under SCFT iteration, in particular when point patterns associated with the local energy minima of the Quantizer energy are used as initial sphere center locations.

Hyperuniformity of Disordered Micelle Mesophases. Next, we ran large-cell SCFT simulations (see Supporting Information for the simulation details) of disordered packings of 2000 A-rich micelles distributed in the B-rich matrix in an initial cell corresponding to $10 \times 10 \times 10$ BCC unit cells in size. In our SCFT simulations, we employed periodic boundary conditions and maintained the box shape to be cubic while allowing the side length of the box to vary, which is consistent with the boundary conditions used to generate the initial point patterns. Mathematically, any mesophase formed by incompressible melts of AB linear diblock copolymers is uniquely specified by the A-block density field $\rho_{\rm A}({\bf r})$ (normalized by the average total monomer density ρ_0), which is a scalar field with values between 0 and 1. Its scattering intensity is proportional to the structure factor S(k) (see Supporting Information for a definition), which can be used to analyze the hyperuniformity of the mesophase. The density field $\rho_B(\mathbf{r})$ is related to $\rho_A(\mathbf{r})$ via $\rho_{\rm B}({\bf r}) = 1 - \rho_{\rm A}({\bf r})$ due to the incompressible melt condition. In the soft-matter physics community, the structure factor S(k) is often referred to as the spectral density $\tilde{\psi}(k)$.

In Figure 1a, we visualize the density field $\rho_A(r)$ of a SCFToptimized mesostructure for a disordered packing of 2000 micelles at $\chi N = 17$ and f = 0.25. The ensemble-averaged S(k)values [see Supporting Information for the detail of S(k)calculation of the mesostructures relaxed by SCFT simulations using the aforementioned wide variety of disordered point patterns as initial micelle centers are shown in Figure 1b, which are averaged over 10 independent starting configurations. We find that all these SCFT simulations lead to very similar final relaxed structures with essentially identical pair statistics, as shown in Figure 1a, and virtually the same free energies. However, SCFT simulations initialized using the point patterns associated with the local energy minima of the Quantizer problem (henceforth referred to as the Quantizer point patterns) were much quicker to converge than those initialized using other disordered point patterns, suggesting that the Quantizer point patterns are far more realistic than the other disordered point patterns for the micelle centers in the melts of AB linear diblock copolymers. Therefore, we used these Quantizer point patterns as initial micelle centers for subsequent SCFT simulations. As a comparison, we also include S(k) for a 10 × 10 × 10 periodic replica of a BCC sphere mesophase in a conventional cell at the same condition. Interestingly, S(k) of the mesophases consisting of disordered micelles possesses a broad primary peak with no other sharp Bragg peaks, indicating the lack of conventional translational and orientational order commonly seen in crystals or quasicrystals. The structure factor S(k) of the BCC sphere, on the other hand, possesses multiple sharp Bragg peaks, as expected. Importantly, S(k) of the disordered micelles approaches zero as k goes to zero; i.e., the corresponding mesophases are hyperuniform, analogous to crystals or quasicrystals. This behavior is different from typical liquids or molecular glasses, where one would expect S(k) to approach some finite value as k approaches zero.² In the present case, the apparent vanishing of S(0) is not a trivial result of the incompressible melt assumption since S(k) reflects only Asegment correlations, not total density correlations. We note that S(k) is on the order of 10^{-9} at the smallest k directly

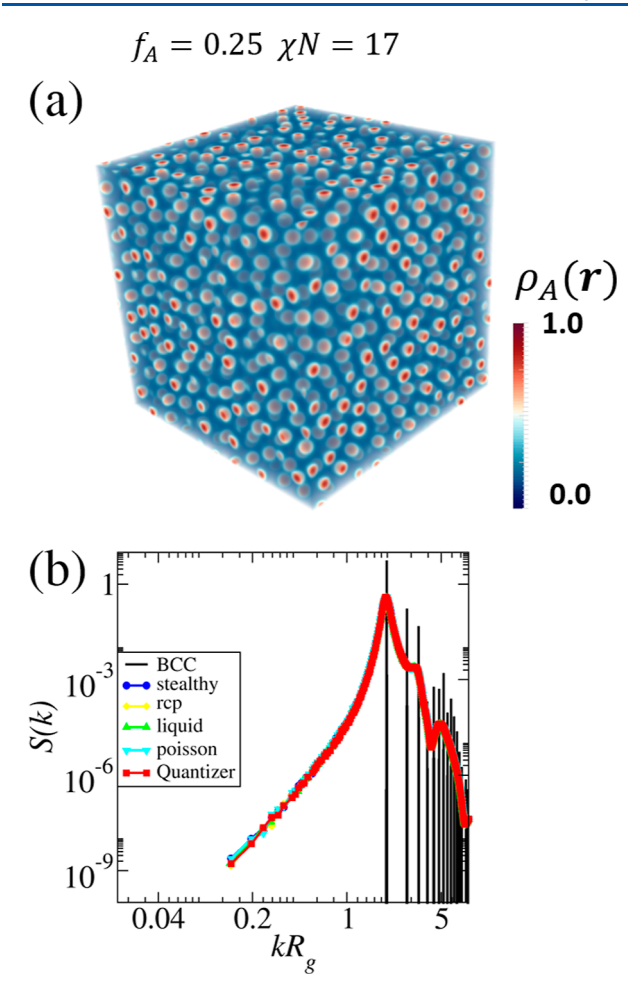


Figure 1. (a) Visualization of the SCFT-solved density field $\rho_A(\mathbf{r})$ of a metastable mesophase consisting of A-rich micelles distributed in a B-rich matrix in neat melts of AB linear diblock copolymers at $\chi N=17$ and $f_A=0.25$. (b) Ensemble-averaged structure factor S(k) of the disordered micelle mesophases resolved by SCFT simulations at $\chi N=17$ and $f_A=0.25$ using different disordered point patterns as initial sphere locations, as well as that of a BCC sphere phase containing 2000 micelles at the same χN and f_A . We consider disordered point patterns such as point configurations of the local energy minima of the Quantizer problem, Poisson point patterns, liquids, random close packings of hard spheres, and disordered hyperuniform stealthy point patterns (see Supporting Information for details).

accessible in our SCFT simulations, indicating a very high degree of hyperuniformity for these mesophases, while the Quantizer point patterns used to seed the SCFT simulations are only effectively hyperuniform, with their S(k) on the order of 10^{-3} at the smallest k. This difference in the degree of hyperuniformity suggests that the local relaxation due to the simultaneous minimization of interfacial area between different domains and chain stretching of block copolymers helps drive the system toward hyperuniformity.

It is also noteworthy that slight polydispersity develops for the micelles in the DHU state as a result of the SCFT relaxation, which contributes to the hyperuniformity of the final micelle structures as well. For example, the polydisperse degree of the micelles measured by $\gamma = r_{\rm max}/r_{\rm min}$ is around 1.2 at $\chi N = 17$ and $f_{\rm A} = 0.25$, where $r_{\rm max}$ and $r_{\rm min}$ are the radii of the largest and smallest micelles, respectively. To determine the radii for different micelles, we first convert the scalar field $\rho_{\rm A}({\bf r})$ into a two-phase media by thresholding $\rho_{\rm A}({\bf r})$, i.e., any spatial

location (or voxel) with $\rho_{\rm A}({\bf r})$ larger than the threshold $\rho_{\rm A,t}$ is considered to be in the A-rich phase/region and otherwise in the B-rich phase/region. The threshold $\rho_{\rm A,t}$ is chosen such that the volume occupied by the A-rich region is the same as that occupied by the A monomers before thresholding. A micelle consists of all the voxels that are in the same interconnected "cluster" of the A-rich phase after thresholding, and the radius of a micelle r_i is computed as $r_i = \left(\frac{3v_i}{4\pi}\right)^{1/3}$, where v_i is the volume of that micelle. Similarly, the center of a micelle can be determined by averaging over the positions of all of the voxels that belong to the micelle. Moreover, the micelles in the DHU mesophase exhibit a broad distribution in the number of neighbors, as shown in Figure 2, where neighboring micelles

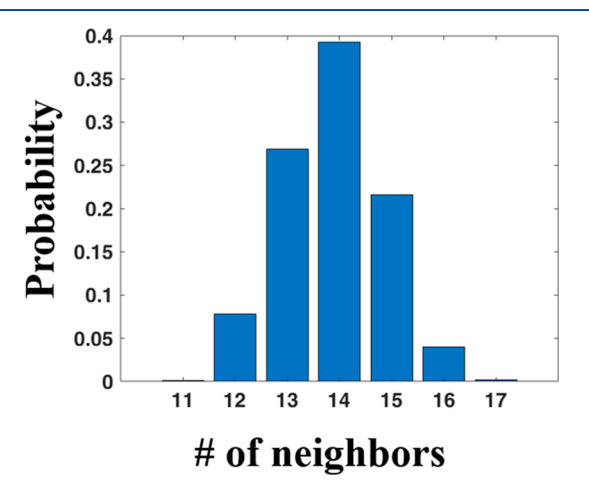


Figure 2. Ensemble-averaged neighbor distribution for micelles in the disordered hyperuniform mesophase at $\chi N=17$ and $f_{\rm A}=0.25$, where neighboring micelles are defined as those whose Voronoi cells share a common facet.

are defined as those whose Voronoi cells (constructed using the Voro++ package 40) share a common facet. In contrast, in the BCC phase, the Voronoi cell of each micelle is a truncated octahedron with exactly 14 neighbors. The DHU mesophase also has a much wider neighbor distribution compared to Frank–Kasper phases. 22,27,41 For instance, micelles in the C14 and C15 phases have either 12 or 16 neighbors, while those in the σ phase have 12, 14, or 15 neighbors. In addition, the average domain spacing between neighboring spheres is swollen by around 1.2% in the DHU state compared to that in the BCC sphere phase, consistent with the observed shift in the location of the primary peak in S(k).

As χN varies at a given $f_{A^{\prime}}$ the morphology of the DHU micelle mesophases also changes. As an example, in Figure 3a, we show S(k) at different χN for $f_A=0.25$, which all indicate hyperuniformity for the corresponding micelle mesophases. We then proceed to determine the small-k scaling exponent α in $S(k) \sim k^{\alpha}$ by looking at the large-t scaling behavior of the excess diffusion spreadability 42,43 $S(\infty)-S(t)$ computed from S(k) (see Supporting Information for details). We find that as χN increases, the exponent α decreases, as shown in Figure 3b, which can be explained by the fact that as χN increases, the A-rich and B-rich regions become purer in A and B, respectively, and the composition fluctuations between A-rich and B-rich domains increase, which dominates the large-wavelength physics and leads to decreasing α . The α values in Figure 3b are also much larger than the scaling exponent $\alpha=2$

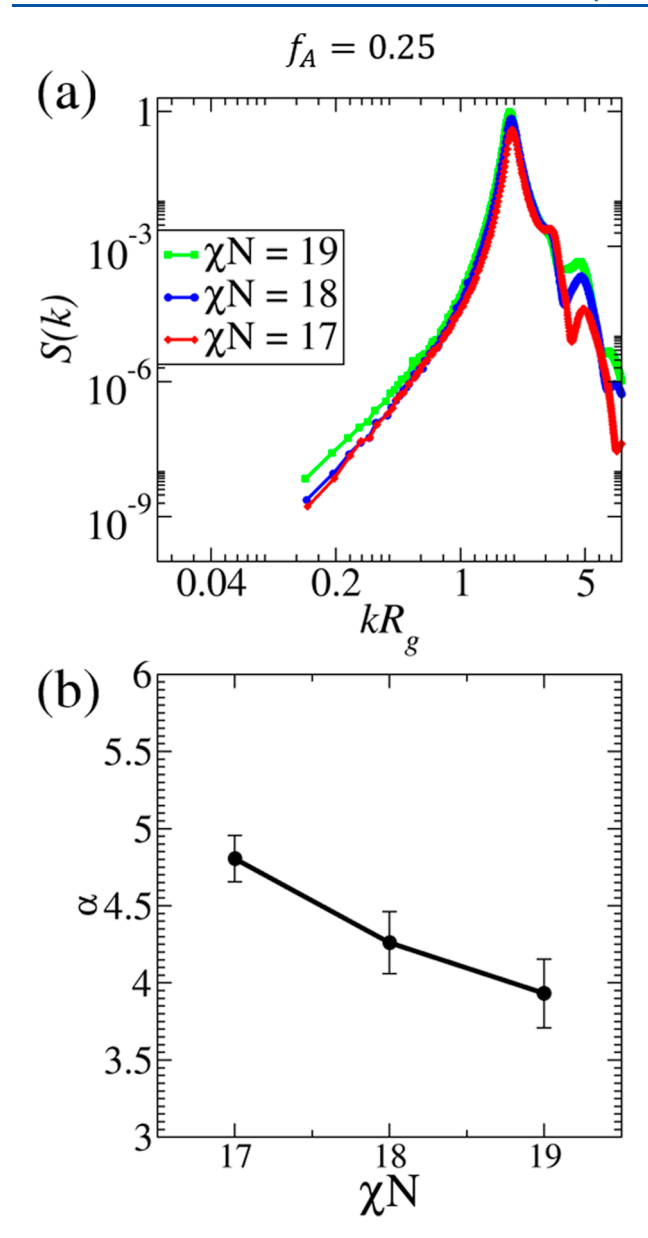


Figure 3. Ensemble-averaged S(k) and the corresponding small-k exponent α in $S(k) \sim k^{\alpha}$ as functions of the segregation strength χN at $f_A = 0.25$ are shown in (a,b), respectively.

predicted by the random phase approximation (RPA). The RPA calculation extracts the linear response of the disordered homogeneous state and is valid only when χN is below $(\chi N)_{\rm ODT}$. Furthermore, the mean distance between neighboring spheres in these mesophases increases by about 3.0% as χN increases from 17 to 19 at $f_{\rm A}=0.25$, as reflected by the shift of the primary peak of S(k) to smaller k, which is accompanied by a proportional increase in the mean size of micelles.

Thermodynamic Stability of Disordered Micelle Mesophases. We now discuss in detail the energetics of the DHU mesophases. In Figure 4a,b, we show the free energy difference between these metastable phases and the global free energy minimum of BCC spheres as a function of segregation strength χN at $f_A=0.20$ and $f_A=0.25$. Interestingly, these DHU micelle mesophases possess very similar free energies to the BCC sphere mesophase. For example, at $\chi N=17$ and $f_A=0.25$, the mean free energy of the DHU micelles is only 1.0×10^{-3} k_BT per chain higher than that of the BCC structure and

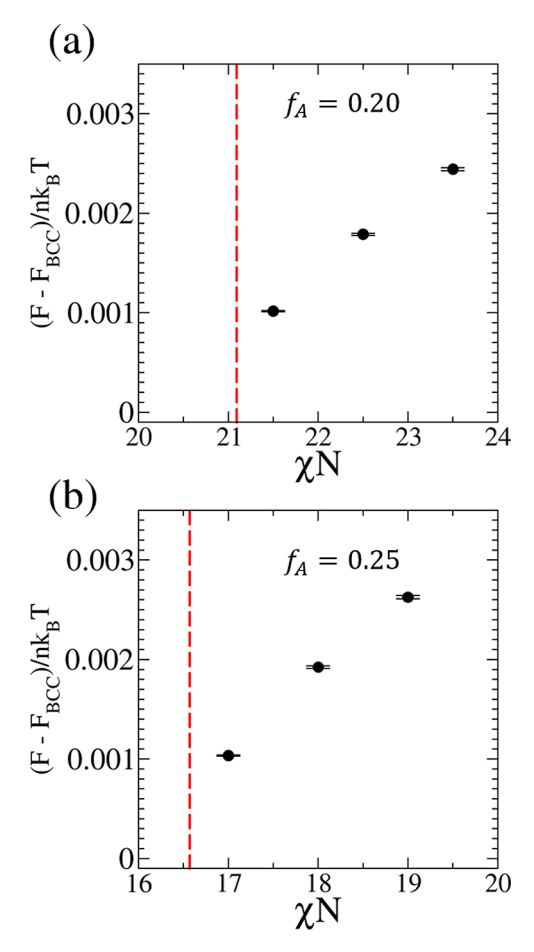


Figure 4. Mean free energy difference between the metastable DHU micelles and the thermodynamically stable BCC sphere mesophase as a function of the segregation strength χN at monomer volume fractions $f_{\rm A}=0.20$ (a) and $f_{\rm A}=0.25$ (b). The red dashed lines indicate $(\chi N)_{\rm ODT}$, where the order–disorder transition between the BCC phase and the disordered homogeneous state occurs.

 $6.8 \times 10^{-3} \ k_{\rm B}T$ per chain lower than the disordered homogeneous state (with free energy 1.0003 \times F_{BCC}), where $k_{\rm B}$ is the Boltzmann constant. By contrast, the mean free energy of the previously obtained 31 disordered fluid-like packings is approximately $2.5 \times 10^{-3} k_B T$ per chain higher than that of the BCC morphology, which is considerably higher than that of our DHU mesophases. In other words, DHU micelles are much more favorable energetically than previously obtained liquid-like packings.³¹ With the state-ofthe-art optimization algorithms that were employed (see Supporting Information for details), all the DHU micelle mesophases obtained after SCFT relaxation at a given χN and f_A possess very similar free energies from different runs, which is different from the sizable distribution of free energies reported in a previous study.³¹ For example, the standard error associated with the free energy is only $5.0 \times 10^{-6} k_B T$ per chain at $\chi N = 17$ and $f_A = 0.25$. It is also noteworthy that, as mentioned in the previous section, even when starting from completely random or fluid initial configurations, we were still able to achieve DHU mesophases that reflect deep local free energy minima, even though the computational effort to relax the structures increased.

We observe that the stability of DHU micelles relative to the BCC phase increases as the segregation strength decreases and approaches the order-disorder transition (ODT), regardless

of the monomer species volume fraction f_A . In particular, the free energy difference between DHU micelles and BCC spheres increases approximately linearly as χN increases away from the ODT. Here, the segregation strength $(\chi N)_{\mathrm{ODT}}$ at the ODT is estimated to be 21.09 and 16.57 for $f_A = 0.20$ and $f_A =$ 0.25, respectively, from SCFT simulations of the disordered homogeneous phase and the BCC sphere mesophase. As the temperature decreases and χN becomes sufficiently large [e.g., $\chi N - (\chi N)_{\rm ODT} \gtrsim 5$ at $f_{\rm A} = 0.20$], the free energy difference between DHU micelles and BCC spheres (scaled by the thermal energy) becomes large enough (close to the free energy difference between BCC spheres and hexagonally packed cylinders) that will make the formation of DHU mesophases difficult. On the other hand, as temperature increases and χN decreases below $(\chi N)_{\rm ODT}$, the system is no longer microphase-separated and becomes trivially homogeneous (in the mean-field approximation of SCFT), which is not interesting for typical applications involving DHU materials. These results indicate that disordered hyperuniform mesophases are most likely to be observed in the disordered micelle regime, 44-46 i.e., at intermediate segregation strengths above the ODT.

Robustness of Results with Respect to System Size and Compressibility. To investigate the effect of the system size on the hyperuniformity and thermodynamic (meta)-stability of the disordered micelle mesophases, we conducted SCFT simulations containing $N_s = 432$ micelles at $\chi N = 17$ and $f_A = 0.25$ and compared the results to the corresponding simulations containing $N_s = 2000$ micelles. The side lengths L of the relaxed cubic SCFT simulation boxes are $L \approx 45.3R_g$ and $L \approx 27.2R_g$ for system sizes $N_s = 2000$ and $N_s = 432$, respectively, where R_g is the unperturbed radius of gyration of a polymer chain. As shown in Figure 5, the structural factors of

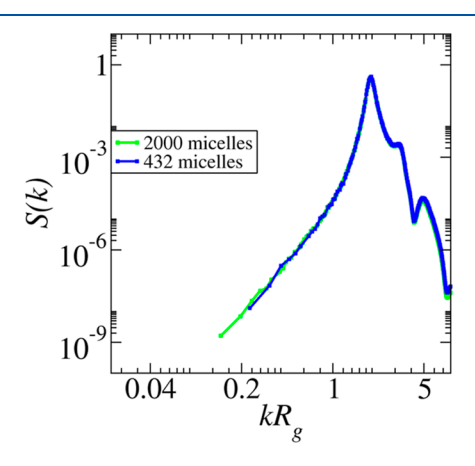


Figure 5. Ensemble-averaged structure factor S(k) of disordered hyperuniform micelle mesophases formed by incompressible melts of linear AB diblock copolymers at $\chi N=17$ and $f_{\rm A}=0.25$ for two different system sizes $N_{\rm s}=2000$ and $N_{\rm s}=432$ micelles (averaged over 10 configurations).

the two systems are consistent with each other, and both systems possess hyperuniformity. Moreover, the mean free energy difference between the final relaxed structures at these two system sizes is only on the order of $1\times 10^{-5}\ k_{\rm B}T$ per chain. These results further demonstrate the robustness of hyperuniformity and thermodynamic (meta)stability of the disordered micelle mesophases investigated in this work with respect to system size.

To investigate the effect of the compressibility of block copolymer melts on the hyperuniformity of disordered micelle mesophases, instead of applying the incompressible melt approximation $\delta[\rho_{\rm A}({\bf r}) + \rho_{\rm B}({\bf r}) - \rho_{\rm 0}]$, we allow the total monomer density to vary spatially and add a quadratic term $\zeta N[\rho_{\rm A}({\bf r}) + \rho_{\rm B}({\bf r}) - \rho_{\rm 0}]^2$ to the Hamiltonian to penalize any total monomer density deviation from the global average at each spatial location, where ζ is the Helfand compressibility coefficient and ζN controls the strength of the penalty. Here, we set $\zeta N=100$, a value used to model moderately compressible melts previously in a previous work. We compare S(k) of compressible melts of linear AB diblock copolymers at $\chi N=17$ and $f_{\rm A}=0.25$ to those of their incompressible counterparts containing 2000 micelles in Figure 6. Even for this modest compressibility, the disordered

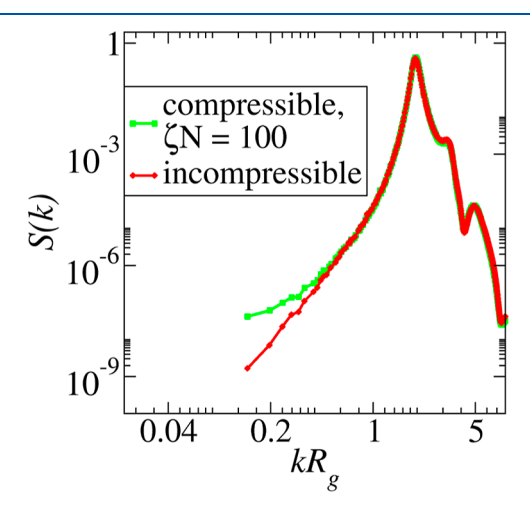


Figure 6. Ensemble-averaged structure factor S(k) of disordered hyperuniform micelle mesophases formed by compressible melts of linear AB diblock copolymers at $\zeta N = 100$ and their corresponding incompressible systems containing 2000 micelles at $\chi N = 17$ and $f_{\rm A} = 0.25$, where ζ is the Helfand compressibility coefficient.

micelle mesophases remain hyperuniform (or at least effectively hyperuniform²) as the ensemble-averaged S(k) still extrapolates to virtually zero as k goes to zero within the accuracy of this study (see Supporting Information for details), but the composition fluctuations are larger compared to those in the corresponding incompressible system.

CONCLUSIONS AND DISCUSSION

To summarize, in this work, we demonstrated the emergence of disordered hyperuniform mesophases in neat melts of sphere-forming block copolymers by conducting SCFT simulations of large systems containing as many as 2000 micelles. Moreover, we showed that these disordered hyperuniform mesophases derived from point configurations corresponding to the local energy minimum of the Quantizer energy possess very similar free energies to the thermodynamically stable BCC structure and are more favorable energetically than previously studied³¹ disordered fluid-like packings. Our findings suggest an inexpensive route to make disordered hyperuniform materials given the wide commercial availability of block copolymers and may lead to new applications. For example, the isotropic nature of the disordered hyperuniform micelle mesophases and their selective scattering of certain wavelengths of electromagnetic waves might enable the design

of novel noniridescent structural colors ⁴⁸ if the distances between the micelles are tuned to optically relevant length scales. This could be facilitated both through polymer architectural design, e.g., moving from linear to bottlebrush block polymers, as well as by the addition of selective solvents. We note that angle-independent structural colors have been realized from disordered colloidal materials, ^{49,50} and tunable angle-dependent structural colors have been achieved using ordered lamellar structures formed by bottlebrush block copolymers. ⁵¹

It is also noteworthy that while we are unaware of experimental evidence suggesting that the observed liquid-like packings ^{25,26} are hyperuniform, given the low free energies of the metastable DHU micelles, it is entirely possible that some of those liquid-like packings will be verified to be DHU in the future. The recent development of high-resolution real-space imaging techniques ^{52–54} for soft-matter systems presents new opportunities for such experiments, where one could directly compute the structure factor or local variance associated with fluctuations in the field ³⁸ from the extracted real-space microstructures and ascertain the hyperuniformity of the mesophases. Moreover, the realization of DHU structures in neat melts of block copolymers might be facilitated by tuning the thermal processing procedures.

DHU micelle mesophases are also similar to the maximally random jamming (MRJ) state⁵⁵ and perfect glass state⁵⁶ in that they reflect deep free energy minima and are hyperuniform. However, unlike the MRJ state and perfect glass state that can never crystallize, 56 our DHU micelle mesophases possess higher free energies than the thermodynamically stable ordered BCC micelle mesophase, and the energy barrier is expected to be finite, so DHU micelle mesophases can crystallize over long periods of time. In addition, the DHU micelle mesophases are realizations of random scalar fields, which differ from the cases of the MRJ state and perfect glass state, where one is dealing with discrete particles. Such a random field, of course, approximates a (soft) sphere packing but with a slight degree of polydispersity as discussed above and can take any value between 0 and 1 instead of a binary value (0 or 1) at a given spatial location. These additional degrees of freedom facilitate the formation of hyperuniform materials similar to the topdown tessellation-based procedure for two-phase media in a previous work.⁵⁷ Here, however, block copolymer selfassembly enables a bottom-up approach.

ASSOCIATED CONTENT

Supporting Information

The Supporting Information is available free of charge at https://pubs.acs.org/doi/10.1021/acs.macromol.4c01807.

Brief introduction to SCFT simulations; details of SCFT simulations; numerical calculation of the structure factor; extrapolation of the structure factor to the infinite wavelength; and numerical calculation of the small-wavenumber scaling exponent for the structure factor (PDF)

AUTHOR INFORMATION

Corresponding Authors

Duyu Chen — Materials Research Laboratory, University of California, Santa Barbara, California 93106, United States; orcid.org/0000-0002-4962-8013; Email: duyu@alumni.princeton.edu

Glenn H. Fredrickson – Materials Research Laboratory, University of California, Santa Barbara, California 93106, United States; Department of Chemical Engineering, University of California, Santa Barbara, California 93106, United States; orcid.org/0000-0002-6716-9017; Email: ghf@mrl.ucsb.edu

Author

Michael A. Klatt – Institut für KI Sicherheit, Deutsches Zentrum für Luft- und Raumfahrt (DLR), Ulm 89081, Germany; Institut für Materialphysik im Weltraum, Deutsches Zentrum für Luft- und Raumfahrt (DLR), Köln 51170, Germany; Department of Physics, Ludwig-Maximilians-Universität, Munich 80799, Germany

Complete contact information is available at: https://pubs.acs.org/10.1021/acs.macromol.4c01807

Notes

The authors declare no competing financial interest.

ACKNOWLEDGMENTS

D.C. and G.H.F. were supported by the U.S. Department of Energy, Office of Basic Energy Sciences, under Award Number DE-SC0019001. This work made use of the BioPACIFIC Materials Innovation Platform computing resources of the National Science Foundation Award No. DMR-1933487. Use was also made of computational facilities purchased with funds from the National Science Foundation (OAC-1925717 and CNS-1725797) and administered by the Center for Scientific Computing (CSC). The CSC is supported by the California NanoSystems Institute and the Materials Research Science and Engineering Center (MRSEC; NSF DMR-2308708) at UC Santa Barbara. M.A.K. acknowledges funding and support by the Deutsche Forschungsgemeinschaft (DFG, German Research Foundation) through SPP 2265, under grant numbers KL 3391/2-2, WI 5527/1-1, and LO 418/25-1, and by the Initiative and Networking Fund of the Helmholtz Association through the Project "DataMat". We also thank Dr. Ge Zhang for supplying us configurations of disordered stealthy hyperuniform point patterns and Dr. Christopher Balzer and Timothy Quah for helpful discussion.

REFERENCES

- (1) Torquato, S.; Stillinger, F. H. Local density fluctuations, hyperuniformity, and order metrics. *Phys. Rev. E* **2003**, *68*, 041113.
- (2) Torquato, S. Hyperuniform states of matter. *Phys. Rep.* **2018**, 745, 1–95.
- (3) Zachary, C. E.; Torquato, S. Hyperuniformity in point patterns and two-phase random heterogeneous media. *J. Stat. Mech.: Theory Exp.* **2009**, 2009, P12015.
- (4) Florescu, M.; Torquato, S.; Steinhardt, P. J. Designer disordered materials with large, complete photonic band gaps. *Proc. Natl. Acad. Sci. U.S.A.* **2009**, *106*, 20658–20663.
- (5) Man, W.; Florescu, M.; Williamson, E. P.; He, Y.; Hashemizad, S. R.; Leung, B. Y. C.; Liner, D. R.; Torquato, S.; Chaikin, P. M.; Steinhardt, P. J. Isotropic band gaps and freeform waveguides observed in hyperuniform disordered photonic solids. *Proc. Natl. Acad. Sci. U.S.A.* **2013**, *110*, 15886–15891.
- (6) Jiao, Y.; Lau, T.; Hatzikirou, H.; Meyer-Hermann, M.; Corbo, J. C.; Torquato, S. Avian photoreceptor patterns represent a disordered hyperuniform solution to a multiscale packing problem. *Phys. Rev. E* **2014**, *89*, 022721.
- (7) Dreyfus, R.; Xu, Y.; Still, T.; Hough, L. A.; Yodh, A. G.; Torquato, S. Diagnosing hyperuniformity in two-dimensional,

- disordered, jammed packings of soft spheres. Phys. Rev. E 2015, 91, 012302.
- (8) Hexner, D.; Levine, D. Hyperuniformity of critical absorbing states. *Phys. Rev. Lett.* **2015**, *114*, 110602.
- (9) Jack, R. L.; Thompson, I. R.; Sollich, P. Hyperuniformity and Phase Separation in Biased Ensembles of Trajectories for Diffusive Systems. *Phys. Rev. Lett.* **2015**, *114*, 060601.
- (10) Zhang, G.; Stillinger, F. H.; Torquato, S. Transport, geometrical, and topological properties of stealthy disordered hyperuniform two-phase systems. *J. Chem. Phys.* **2016**, *145*, 244109.
- (11) Rumi, G.; Sánchez, J. A.; Elías, F.; Maldonado, R. C.; Puig, J.; Bolecek, N. R. C.; Nieva, G.; Konczykowski, M.; Fasano, Y.; Kolton, A. B. Hyperuniform vortex patterns at the surface of type-II superconductors. *Phys. Rev. Res.* **2019**, *1*, 033057.
- (12) Huang, M.; Hu, W.; Yang, S.; Liu, Q.-X.; Zhang, H. P. Circular swimming motility and disordered hyperuniform state in an algae system. *Proc. Natl. Acad. Sci. U.S.A.* **2021**, *118*, e2100493118.
- (13) Lei, Q.-L.; Ciamarra, M. P.; Ni, R. Nonequilibrium strongly hyperuniform fluids of circle active particles with large local density fluctuations. *Sci. Adv.* **2019**, *5*, eaau7423.
- (14) Lei, Q.-L.; Ni, R. Hydrodynamics of random-organizing hyperuniform fluids. *Proc. Natl. Acad. Sci. U.S.A.* **2019**, *116*, 22983–22989.
- (15) Xu, Y.; Chen, S.; Chen, P.; Xu, W.; Jiao, Y. Microstructure and mechanical properties of hyperuniform heterogeneous materials. *Phys. Rev. E* **2017**, *96*, 043301.
- (16) Klatt, M. A.; Steinhardt, P. J.; Torquato, S. Wave Propagation and Band Tails of Two-Dimensional Disordered Systems in the Thermodynamic Limit. *Proc. Natl. Acad. Sci. U.S.A.* **2022**, *119*, e2213633119
- (17) Chehadi, Z.; Bouabdellaoui, M.; Modaresialam, M.; Bottein, T.; Salvalaglio, M.; Bollani, M.; Grosso, D.; Abbarchi, M. Scalable disordered hyperuniform architectures via nanoimprint lithography of metal oxides. *ACS Appl. Mater. Interfaces* **2021**, *13*, 37761–37774.
- (18) Salvalaglio, M.; Bouabdellaoui, M.; Bollani, M.; Benali, A.; Favre, L.; Claude, J.-B.; Wenger, J.; de Anna, P.; Intonti, F.; Voigt, A.; Abbarchi, M. Hyperuniform monocrystalline structures by spinodal solid-state dewetting. *Phys. Rev. Lett.* **2020**, *125*, 126101.
- (19) Chremos, A.; Douglas, J. F. Hidden hyperuniformity in soft polymeric materials. *Phys. Rev. Lett.* **2018**, *121*, 258002.
- (20) Klatt, M. A.; Lovrić, J.; Chen, D.; Kapfer, S. C.; Schaller, F. M.; Schönhöfer, P. W. A.; Gardiner, B. S.; Smith, A.; Schröder-Turk, G. E.; Torquato, S. Universal hidden order in amorphous cellular geometries. *Nat. Commun.* **2019**, *10*, 811.
- (21) Grason, G. M.; DiDonna, B. A.; Kamien, R. D. Geometric theory of diblock copolymer phases. *Phys. Rev. Lett.* **2003**, *91*, 058304.
- (22) Reddy, A.; Buckley, M. B.; Arora, A.; Bates, F. S.; Dorfman, K. D.; Grason, G. M. Stable Frank—Kasper phases of self-assembled, soft matter spheres. *Proc. Natl. Acad. Sci. U.S.A.* **2018**, *115*, 10233—10238.
- (23) Bates, F. S.; Fredrickson, G. H. Block copolymer thermodynamics: theory and experiment. *Annu. Rev. Phys. Chem.* **1990**, *41*, 525–557.
- (24) Bates, F. S.; Fredrickson, G. H. Block copolymers—designer soft materials. *Phys. Today* **1999**, *52*, 32–38.
- (25) Bates, C. M.; Bates, F. S. 50th Anniversary Perspective: Block Polymers- Pure Potential. *Macromolecules* **2017**, *50*, 3–22.
- (26) Lodge, T. P.; Seitzinger, C. L.; Seeger, S. C.; Yang, S.; Gupta, S.; Dorfman, K. D. Dynamics and Equilibration Mechanisms in Block Copolymer Particles. *ACS Polym. Au* **2022**, *2*, 397–416.
- (27) Kim, K.; Schulze, M. W.; Arora, A.; Lewis, R. M.; Hillmyer, M. A.; Dorfman, K. D.; Bates, F. S. Thermal processing of diblock copolymer melts mimics metallurgy. *Science* **2017**, *356*, 520–523.
- (28) Kim, K.; Arora, A.; Lewis, R. M.; Liu, M.; Li, W.; Shi, A.-C.; Dorfman, K. D.; Bates, F. S. Origins of low-symmetry phases in asymmetric diblock copolymer melts. *Proc. Natl. Acad. Sci. U.S.A.* **2018**, *115*, 847–854.
- (29) Gillard, T. M.; Lee, S.; Bates, F. S. Dodecagonal quasicrystalline order in a diblock copolymer melt. *Proc. Natl. Acad. Sci. U.S.A.* **2016**, *113*, 5167–5172.

- (30) Bates, M. W.; Barbon, S. M.; Levi, A. E.; Lewis, R. M., III; Beech, H. K.; Vonk, K. M.; Zhang, C.; Fredrickson, G. H.; Hawker, C. J.; Bates, C. M. Synthesis and self-assembly of AB_n miktoarm star polymers. *ACS Macro Lett.* **2020**, *9*, 396–403.
- (31) Dorfman, K. D.; Wang, Z.-G. Liquid-Like States in Micelle-Forming Diblock Copolymer Melts. *ACS Macro Lett.* **2023**, *12*, 980–985.
- (32) Yadav, M.; Bates, F. S.; Morse, D. C. Network model of the disordered phase in symmetric diblock copolymer melts. *Phys. Rev. Lett.* 2018, 121, 127802.
- (33) Fredrickson, G. H. The Equilibrium Theory of Inhomogeneous Polymers; Oxford University Press: Oxford, 2006.
- (34) Düchs, D.; Delaney, K. T.; Fredrickson, G. H. A multi-species exchange model for fully fluctuating polymer field theory simulations. *J. Chem. Phys.* **2014**, *141*, 174103.
- (35) Du, Q.; Faber, V.; Gunzburger, M. Centroidal Voronoi Tessellations: Applications and Algorithms. SIAM Rev. 1999, 41, 637–676.
- (36) Skoge, M.; Donev, A.; Stillinger, F. H.; Torquato, S. Packing hyperspheres in high-dimensional Euclidean spaces. *Phys. Rev. E* **2006**, 74, 041127.
- (37) Torquato, S.; Zhang, G.; Stillinger, F. H. Ensemble theory for stealthy hyperuniform disordered ground states. *Phys. Rev. X* **2015**, *5*, 021020.
- (38) Torquato, S. Hyperuniformity and its generalizations. *Phys. Rev.* E **2016**, 94, 022122.
- (39) Ma, Z.; Torquato, S. Random Scalar Fields and Hyper-uniformity. J. Appl. Phys. 2017, 121, 244904.
- (40) Rycroft, C. VORO++: A three-dimensional Voronoi cell library in C++. *Chaos* **2009**, *19*, 041111.
- (41) Su, Z.; Hsu, C.-H.; Gong, Z.; Feng, X.; Huang, J.; Zhang, R.; Wang, Y.; Mao, J.; Wesdemiotis, C.; Li, T.; Seifert, S.; Zhang, W.; Aida, T.; Huang, M.; Cheng, S. Z. D. Identification of a Frank–Kasper Z phase from shape amphiphile self-assembly. *Nat. Chem.* **2019**, *11*, 899–905.
- (42) Wang, H.; Torquato, S. Dynamic measure of hyperuniformity and nonhyperuniformity in heterogeneous media via the diffusion spreadability. *Phys. Rev. Appl.* **2022**, *17*, 034022.
- (43) Hitin-Bialus, A.; Maher, C. E.; Steinhardt, P. J.; Torquato, S. Hyperuniformity classes of quasiperiodic tilings via diffusion spreadability. *Phys. Rev. E* **2024**, *109*, 064108.
- (44) Dormidontova, E. E.; Lodge, T. P. The order-disorder transition and the disordered micelle regime in sphere-forming block copolymer melts. *Macromolecules* **2001**, *34*, 9143–9155.
- (45) Wang, J.; Wang, Z.-G.; Yang, Y. Nature of disordered micelles in sphere-forming block copolymer melts. *Macromolecules* **2005**, 38, 1979–1988.
- (46) Chawla, A.; Bates, F. S.; Dorfman, K. D.; Morse, D. C. Identifying a critical micelle temperature in simulations of disordered asymmetric diblock copolymer melts. *Phys. Rev. Mater.* **2021**, *5*, L092601.
- (47) Delaney, K. T.; Fredrickson, G. H. Recent developments in fully fluctuating field-theoretic simulations of polymer melts and solutions. *J. Phys. Chem. B* **2016**, *120*, 7615–7634.
- (48) Yu, S.; Qiu, C.-W.; Chong, Y.; Torquato, S.; Park, N. Engineered disorder in photonics. *Nat. Rev. Mater.* **2020**, *6*, 226–243.
- (49) Hwang, V.; Stephenson, A. B.; Barkley, S.; Brandt, S.; Xiao, M.; Aizenberg, J.; Manoharan, V. N. Designing angle-independent structural colors using Monte Carlo simulations of multiple scattering. *Proc. Natl. Acad. Sci. U.S.A.* **2021**, *118*, e2015551118.
- (50) Demirörs, A. F.; Poloni, E.; Chiesa, M.; Bargardi, F. L.; Binelli, M. R.; Woigk, W.; de Castro, L. D. C.; Kleger, N.; Coulter, F. B.; Sicher, A.; Galinski, H.; Scheffold, F.; Studart, A. R. Three-dimensional printing of photonic colloidal glasses into objects with isotropic structural color. *Nat. Commun.* **2022**, *13*, 4397.
- (51) Patel, B. B.; Walsh, D. J.; Kim, D. H.; Kwok, J.; Lee, B.; Guironnet, D.; Diao, Y. Tunable structural color of bottlebrush block copolymers through direct-write 3D printing from solution. *Sci. Adv.* **2020**, *6*, eaaz7202.

- (52) Yang, Y.; Zhou, J.; Zhu, F.; Yuan, Y.; Chang, D. J.; Kim, D. S.; Pham, M.; Rana, A.; Tian, X.; Yao, Y.; Osher, S. J.; Schmid, A. K.; Hu, L.; Ercius, P.; Miao, J. Determining the three-dimensional atomic structure of an amorphous solid. *Nature* **2021**, *592*, 60–64.
- (53) Kang, H. S.; Park, C.; Eoh, H.; Lee, C. E.; Ryu, D. Y.; Kang, Y.; Feng, X.; Huh, J.; Thomas, E. L.; Park, C. Visualization of nonsingular defect enabling rapid control of structural color. *Sci. Adv.* **2022**, 8, eabm5120.
- (54) Subramanian, V.; Wu, K.; Feng, X.; Tsai, E.; Li, R.; Freychet, G.; Zhernenkov, M.; Sen, A.; Mcintosh, A.; Thomas, E. L. Cryo-FIB and Synchrotron SAXS/WAXS Studies of Confined Crystallization of PDMS in Tubular Network Block Copolymer Morphologies. *Microsc. Microanal.* 2023, 29, 523–525.
- (55) Maher, C. E.; Jiao, Y.; Torquato, S. Hyperuniformity of maximally random jammed packings of hyperspheres across spatial dimensions. *Phys. Rev. E* **2023**, *108*, 064602.
- (56) Zhang, G.; Stillinger, F. H.; Torquato, S. The perfect glass paradigm: Disordered hyperuniform glasses down to absolute zero. *Sci. Rep.* **2016**, *6*, 36963.
- (57) Kim, J.; Torquato, S. New tessellation-based procedure to design perfectly hyperuniform disordered dispersions for materials discovery. *Acta Mater.* **2019**, *168*, 143–151.